Iterative Reconstruction
of the Transducer Surface Velocity

Erwin J. Alles and Koen W.A. van Dongen

Abstract—Ultrasound arrays used for medical imaging consist of many elements placed closely together. Ideally, each element vibrates independently. However, due to mechanical coupling, cross-talk between neighboring elements may occur. To quantify the amount of cross-talk, the transducer velocity distribution should be measured.

In this work, a method is presented to reconstruct the velocity distribution from far-field pressure field measurements acquired over an arbitrary surface. The distribution is retrieved from the measurements by solving an integral equation, derived from the Rayleigh integral of the first kind, using a conjugate gradient inversion scheme. This approach has the advantages that it allows for arbitrary transducer and pressure field measurement geometries, as well as the application of regularisation techniques.

Numerical experiments show that measuring the pressure field along a hemisphere enclosing the transducer yields significantly more accurate reconstructions than measuring along a parallel plane. In addition, it is shown that an increase in accuracy is achieved when the assumption is made that all points on the transducer surface vibrate in phase.

Finally, the method has been tested on an actual transducer with an active element of $700\,\mu\mathrm{m} \times 200\,\mu\mathrm{m}$ which operates at a center frequency of 12.2 MHz. For this transducer, the velocity distribution has been reconstructed accurately to within $50\,\mu\mathrm{m}$ precision from pressure measurements at a distance of 1.98 mm ($= 16\lambda_0$) using a $200\,\mu\mathrm{m}$ diameter needle hydrophone.

I. INTRODUCTION

Diagnostic medical ultrasound utilises transducer arrays with large numbers of small elements. These elements may have dimensions down to hundreds of micrometers, and operate at frequencies in the MHz range. Since these small elements are placed closely together, they suffer from mechanical cross-talk, which may deteriorate the image quality. Quantifying the amount of cross-talk requires accurate knowledge of the normal component of the velocity distribution of the transducer surface [1], [2], which is from here on referred to as the "velocity distribution".

Direct measurement of the velocity distribution is complicated: accelerometers and other contact methods disturb the distribution due to inertia [3], and laser Doppler vibrometry [4] requires specialised and expensive hardware to measure vibrations with frequencies of 20 MHz and above, and at a spatial resolution of 20 μm or less. To avoid these complications, and to enable measurements under realistic conditions (e.g. on transducers submerged in water), an indirect method is preferred where the radiated pressure, measured some distance away from the transducer, is used.

Erwin Alles and Koen van Dongen are with the Laboratory of Acoustical Wavefield Imaging, faculty of Applied Sciences, Delft University of Technology, Delft, the Netherlands. E-mail: (E.J.Alles, K.W.A.vanDongen)@TUDelft.nl.

With the indirect approach, pressure field measurements are back-propagated to the transducer surface to reconstruct the velocity distribution. When measurements are taken in a planar domain parallel to the planar transducer surface, back-propagation can be performed analytically using Weyl's representation of the Green's function [5], [6], [7], [8], [9]. Alternatively, time-reversal techniques can be applied, either in the spatial domain [10], [11] or in the wave number domain [12], [13], [14] to reconstruct the velocity distribution. These time-reversal techniques are called (near-field) acoustic holography and are, similar to their counterparts in electromagnetism [15], typically limited to certain simple geometric shapes for both the transducer surface and pressure measurement domain [16].

To extend the validity of acoustic holography to arbitrary geometries for both the pressure measurement domain and the transducer surface, boundary element method-based acoustic holography has been developed, where the sound radiating surface is divided into a number of surfaces of which the contribution to the resulting pressure field is computed using the Kirchhoff integral. By inverting the matrix governing the pressure contribution from each surface element, the transducer velocity can be obtained. This matrix inversion can be performed directly [17] or iteratively [18], [19]. The above methods have all successfully been applied to larger scale situations ranging from complete airplanes [20] to refridgerator compressor engines [21].

Application to ultrasound transducers has been limited to planar transducer surfaces where the pressure is measured along a plane parallel to the transducer surface [12], [14], [10], [11]. However, in (medical) imaging arrays, the elements are typically of dimensions comparable to the wavelength, and consequently have wide radiation patterns. Therefore, to obtain accurate reconstructions, the planar measurement domain need to be inhibitively large to capture energy propagating under large angles. However, sensitivity limitations of the measurement setup limit the maximum dimensions of the measurement plane, and hence the accuracy of the reconstruction.

In this work, a frequency-domain velocity distribution reconstruction method is presented in which the reconstruction problem is viewed as an inverse problem, similar to the boundary element method-based approach. Here, the computationally less expensive Rayleigh integral rather than the Kirchhoff integral is used to express the known measured pressure field as the result of a convolution of an unknown velocity distribution with a known Green's function. By formulating the back-propagation as an inversion problem, a greater flexibility is achieved, as it allows for arbitrary geometries for both the transducer surface and the pressure field measurement
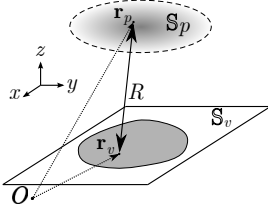
Fig. 1. Sketch of the geometry used. An arbitrarily shaped transducer (gray) is located in the planar domain $\mathbb{S}_v$ and generates a pressure field which is measured in the arbitrarily shaped domain $\mathbb{S}_p$. R is the distance between a point $\mathbf{r}_v$ on the transducer surface and the pressure measurement point $\mathbf{r}_p$.

domain. In this work, the effect of the geometry of the pressure measurement domain on the reconstruction result is studied.

In addition, iterative inversion methods allow for the application of regularisation techniques to further improve the velocity distribution reconstructions. In fact, in most cases regularisation is required [18], [19] to suppress the effect of noise in the measurement on the reconstruction. In this work, regularisation is applied by splitting the velocity distribution into its temporal and spatial parts, where a constant phase over the transducer surface is assumed. In [22] this decomposition is performed to prove uniqueness of the obtained inversion result rather than to improve the result.

In the remainder of this work, first the theory will be treated, followed by synthetic and actual experiments on small transducer elements of 700 μm by 200 μm operating at a center frequency of 12.2 MHz. Both the unregularised inverse problem and the inverse problem assuming constant phase are solved using both a planar and a hemispherical pressure field measurement geometry. In this work, only a single element placed in a planar surface is considered, but the method can equally well be applied to phased and/or steered arrays on arbitrary (curved) domains.

II. THEORY

Consider the geometry shown in figure 1. Here, an arbitrary velocity distribution, located in the planar domain $\mathbb{S}_v$, generates a pressure field $p(\mathbf{r}_p, \omega)$, which is measured in the arbitrarily shaped domain $\mathbb{S}_p$. The pressure field $p(\mathbf{r}_p, \omega)$ can be computed in the frequency domain using the Rayleigh integral of the first kind [23],

$$p(\mathbf{r}_p, \omega) = 2i\omega\rho_0 \int\limits_{\mathbf{r}_v \in \mathbb{S}_v} v_n(\mathbf{r}_v, \omega)\frac{e^{-ik_0 R}}{4\pi R}\mathrm{d}A(\mathbf{r}_v), \quad (1)$$

where ω is the angular frequency, ρ_0 is the volume density of mass of the medium surrounding the transducer, k_0 is the wave number in the surrounding medium, $v_n(\mathbf{r}_v, \omega)$ is the component of the fluid particle velocity normal to the surface $\mathbb{S}_v$, and R is the distance between a source point $\mathbf{r}_v \in \mathbb{S}_v$ and a measurement point $\mathbf{r}_p \in \mathbb{S}_p$. For locally instantaneously reacting fluid, the normal component of the particle velocity of the medium at the transducer surface is equal to that of the transducer surface velocity. As both velocities equal each other, both will from here on be referred to as the velocity distribution $v_n(\mathbf{r}_v, \omega)$.

Equation (1) reads, in operator notation,

$$p(\mathbf{r}_p, \omega) = \mathcal{R}(\mathbf{r}_v, \mathbf{r}_p, \omega)\left[v_n(\mathbf{r}_v, \omega)\right], \quad (2)$$

where $\mathcal{R}(\mathbf{r}_v, \mathbf{r}_p, \omega)$ is the Rayleigh operator. This operator contains the convolution and all scalar multiplications required to obtain pressure $p(\mathbf{r}_p, \omega)$ from the velocity distribution. For known pressure field $p(\mathbf{r}_p, \omega)$ and unknown velocity distribution $v_n(\mathbf{r}_v, \omega)$, equation (2) represents an integral equation of the first kind. This equation represents an inverse problem that is solved using a conjugate gradient (CG) scheme [24], see algorithm 1. As operator $\mathcal{R}(\mathbf{r}_v, \mathbf{r}_p, \omega)$ is not symmetric, CG is applied to the normal equation, which minimises the normalised error functional $E^{(j)}(\omega)$ for each frequency. At the j-th iteration this functional equals

$$E^{(j)}(\omega) = \frac{\sum\limits_{\mathbf{r}_v \in \mathbb{S}_p}\left|\mathcal{R}^* p(\mathbf{r}_p, \omega) - \mathcal{R}^*\mathcal{R}\left[v_n^{(j)}(\mathbf{r}_v, \omega)\right]\right|^2}{\sum\limits_{\mathbf{r}_v \in \mathbb{S}_p}\left|\mathcal{R}^* p(\mathbf{r}_p, \omega)\right|^2} \quad (3)$$

where the summations run over all discrete values of $\mathbf{r}_v \in \mathbb{S}_p$, and $\mathcal{R}^*$ is the adjoint of Rayleigh operator $\mathcal{R}$.

Algorithm 1 The CG scheme on the normal equation

$\mathbf{v}_n^0 = \mathbf{0}$
$\mathbf{d}^0 = \mathbf{r}^0 = \mathcal{R}^*\mathbf{p} - \mathcal{R}^*\mathcal{R}\mathbf{v}_n^0$
$j = 0$
while $j \leq j_{\max}$ and $\frac{\mathbf{r}^j \cdot \mathbf{r}^j}{\mathbf{p} \cdot \mathbf{p}} \geq \epsilon^2$ **do**
$\quad \alpha^j = \frac{\mathbf{r}^j \cdot \mathbf{r}^j}{\mathcal{R}\mathbf{d}^j \cdot \mathcal{R}\mathbf{d}^j}$
$\quad \mathbf{v}_n^{j+1} = \mathbf{v}_n^j + \alpha^j \mathbf{d}^j$
$\quad \mathbf{r}^{j+1} = \mathbf{r}^j - \alpha^j \mathcal{R}^*\mathcal{R}\mathbf{d}^j$
$\quad \mathbf{d}^{j+1} = \mathbf{r}^{j+1} + \frac{\mathbf{r}^{j+1} \cdot \mathbf{r}^{j+1}}{\mathbf{r}^j \cdot \mathbf{r}^j}\mathbf{d}^j$
$\quad j = j + 1$
end while

Applying a CG scheme does not impose any restrictions on the geometries of the spatial domains $\mathbb{S}_v$ and $\mathbb{S}_p$, and in addition allows for the application of regularisation techniques. In contrast, using Weyl's representation of the Green's function requires parallel planer geometries for both the pressure measurement and velocity distribution domains [8]. In this work, full advantage is made of both the flexibility in the geometries of the spatial domains and the ability to apply regularisation techniques.

A. Pressure Measurement Geometry

Most analytical methods use measurements taken in a planar domain $\mathbb{S}_p$ parallel to the surface of the transducer, thereby omitting the acoustic energy radiated under large angles with respect to the normal of the transducer. In general, this approach results in strong spatial smoothening which limits the reconstruction accuracy. This smoothening is the result of the fact that the applied elements are typically smaller than one wavelength, resulting in omni-directional radiation patterns. Consequently, a significant amount of the radiated field propagates outside the finite-sized, planar measurement surface, and is hence not available for reconstruction.

Fortunately, the presented iterative solution method puts no restrictions on the spatial domain $\mathbb{S}_p$ for the measurements. Taking advantage of this, measurements made over the surface of a hemisphere are employed to improve the reconstruction. Compared to a planar domain, a hemisphere has the advantage that it encloses the entire half-space insonified by the source and thereby captures more acoustic energy. In addition, it measures all the acoustic waves at an almost identical distance from the center of the source, thereby retaining the pressure amplitude. Consequently, the resulting velocity distribution reconstruction is expected to be significantly more accurate than in the case of a planar pressure measurement domain.

B. Regularisation

The convergence of the iterative scheme and the accuracy of the reconstructed velocity distribution may be improved by the application of regularisation techniques [25]. In medical acoustical imaging, total variation [26], [27], [28] is a well known regularisation technique used to suppress noise in the reconstruction. However, a drawback of this approach is that it typically leads to smoothening, whereas the results presented later on show that for the velocity distribution reconstruction the opposite is needed.

Alternatively, prior knowledge on the signature of the source signal may be used for regularisation. In the absence of cross-talk, only the excited area of the transducer plane will vibrate. Therefore, if only a single transducer element is present, or if all elements in an array are excited with the same excitation signal, all points on the transducer surface will either oscillate in phase with the same source signature, or not oscillate at all. Consequently, the velocity distribution can be separated in a spatial and a frequency component, i.e.,

$$v_n(\mathbf{r}_v, \omega) = S(\omega)v_0(\mathbf{r}_v), \tag{4}$$

where $S(\omega)$ is the source signal and $v_0(\mathbf{r}_v)$ is the spatially varying velocity distribution amplitude. Combining equation (2) and (4) results in an integral equation of the form

$$p(\mathbf{r}_p, \omega) = \mathcal{R}'(\mathbf{r}_v, \mathbf{r}_p, \omega)\left[v_0(\mathbf{r}_v)\right], \tag{5}$$

where the operator $\mathcal{R}'(\mathbf{r}_v, \mathbf{r}_p, \omega)$ includes the source signature, i.e.,

$$\mathcal{R}'(\mathbf{r}_v, \mathbf{r}_p, \omega) = \mathcal{R}(\mathbf{r}_v, \mathbf{r}_p, \omega)S(\omega). \tag{6}$$

To reconstruct the spatially varying amplitude $v_0(\mathbf{r}_v)$, the applied CG scheme will minimise the normalized error functional $E'^{(j)}(\omega)$, which equals

$$E'^{(j)}(\omega) = \frac{\sum\limits_{\mathbf{r}_v \in \mathbb{S}_p} \left| \mathcal{R}'^* p(\mathbf{r}_p, \omega) - \mathcal{R}'^*\mathcal{R}'\left[v_0^{(j)}(\mathbf{r}_v, \omega)\right] \right|^2}{\sum\limits_{\mathbf{r}_v \in \mathbb{S}_p} \left|\mathcal{R}'^* p(\mathbf{r}_p, \omega)\right|^2}. \tag{7}$$

This regularisation technique is able to reconstruct edges in the original velocity distribution more sharply and hence should reduce spatial smoothening even further. This technique will from here on be referred to as regularisation under constant phase. Note that $v_0(\mathbf{r}_v)$ is frequency independent, and that the source signal $S(\omega)$ needs to be estimated from, e.g., the applied electrical excitation or the result of unregularised CG inversion.

III. EXPERIMENTS

All simulations and reconstructions in this work have been performed in the temporal frequency domain across the entire spectrum. To evaluate the performance of the proposed techniques, the frequency-domain velocity distributions are transformed to the time domain using Fast Fourier transforms.

The described velocity reconstruction technique is tested on synthetic and real pressure field measurements. In all experiments the pressure field is generated by a single transducer element of dimensions 700 μm × 200 μm. The elements are excited by a Gaussian modulated pulse $S(t)$ given by, in the time domain,

$$S(t) = A_0 \cos(2\pi f_0 t)e^{-\frac{(t-\mu)^2}{2\sigma^2}}, \tag{8}$$

with time coordinate t, temporal width $\sigma = 100$ ns, temporal offset $\mu = 200$ ns, center frequency $f_0 = 12.2$ MHz, and velocity amplitude $A_0 = 1$ m/s or voltage amplitude $A_0 = 5$ V for the synthetic and real measurements, respectively. The transducer is placed centrally in a square domain of 2.05 mm × 2.05 mm, divided into 41×41 points each spaced 50 μm apart. The background medium is in all cases water ($c_0 = 1500$ m/s, $\rho_0 = 1000$ kg/m^3).

Measurements are taken in both a plane parallel to the plane $\mathbb{S}_v$ at a distance $z = 1.98$ mm $(= 16\lambda_0)$ and on the surface of a hemisphere of radius $a = 1.98$ mm. The planar domain has dimensions of 2.05 mm × 2.05 mm, divided into 41×41 points each spaced 50 μm apart, resulting in 1681 A-scans. Approximately the same number of A-scans (1654) have been used for the hemispherical domain, and are distributed such that each grid point corresponds to an equal area. Each A-scan contains 301 time samples, sampled at a temporal sampling frequency of 200 MHz. The wavelength corresponding to the center frequency of the applied source signal is $\lambda_0 = 123$ μm, and thus both geometries are in the far-field ($z = a = 16\lambda_0$). The A-scans are computed by first evaluating the frequency domain Rayleigh integral given in equation (1) followed by a Fourier transformation to obtain the resulting time-domain A-scans. The applied CG scheme is stopped when the error functional reaches a level of $E^{(j)} \leq 10^{-2}$. Experiments not treated here showed that a lower $E^{(j)}$ deteriorates the reconstruction result due to overfitting of noise.

A. Synthetic measurements

For the synthetic experiments, a single active transducer is used. The synthetic experiments are performed to quantify the accuracy of the methods. To this aim, the frequency-domain velocity distribution reconstruction $v_n^{(j)}(\mathbf{r}_v, \omega)$ is transformed to the time domain yielding $v_n(\mathbf{r}_v, t)$. The resulting time-domain reconstructions are subsequently used to evaluate the normalised construction error ϵ computed by

$$\epsilon = \frac{\sum\limits_{\mathbf{r}_v \in \mathbb{S}_v} \sum\limits_t \left[v_n(\mathbf{r}_v, t) - v_n^{\text{orig}}(\mathbf{r}_v, t)\right]^2}{\sum\limits_{\mathbf{r}_v \in \mathbb{S}_v} \sum\limits_t \left[v_n^{\text{orig}}(\mathbf{r}_v, t)\right]^2}, \tag{9}$$

where the summations run over all discrete spatiotemporal samples, and with $v_n^{\text{orig}}(\mathbf{r}_v, t)$ the original velocity distribution.

Synthetic measurements in a parallel plane

First, reconstructions using noise-free measurements taken in a planar domain parallel to transducer surface are considered. In figure 2, the same snapshot of the original time-domain velocity distribution and of reconstructions obtained with the unregularised and regularised CG inversion are shown. Note that a vibrating area of approximately the correct dimensions is obtained with both methods, and that the recovered amplitudes are correct. The shown snapshot coincides with the maximum amplitude of the driving Gaussian modulated pulse of equation (8), but the differences between the original and the two reconstructed velocity distributions are of similar relative magnitude in all snapshots.

Both methods suffer from spatial smoothening of similar magnitude, and judging from figure 2, assuming a spatially invariant phase does not seem to improve the reconstruction. In fact, when computing the normalised reconstruction error ϵ of equation (9), the error increases from $\epsilon = 36.0$ % for the full CG inversion to $\epsilon = 49.9$ % for the regularised approach.

By studying the transient behaviour of the velocity distributions, it was observed that the spatial spreading of vibrational energy is reduced by applying constant phase regularisation. This is demonstrated in figure 3, where instead of a single snapshot, the quantity $K(\mathbf{r}_v)$ is given,

$$K(\mathbf{r}_v) = \sum_t \left[v'_n(\mathbf{r}_v, t) \right]^2, \tag{10}$$

which is proportional to the kinetic energy in each point $\mathbf{r}_v$. From this figure it is clear that, despite the larger error in the reconstruction, assuming a constant phase reduces the spatial spreading of the energy and yields a vibrating region that is more sharply defined.

Next, the effect of noise on the reconstruction is demonstrated. To this aim, 5 % white noise, relative to the overall maximum amplitude in the computed pressure fields, is added to the same synthetically measured field $p(\mathbf{r}_p, t)$ as used above. The resulting reconstruction of the kinetic energy distribution $K(\mathbf{r}_v)$ is shown in figure 4. While the unregularised CG inversion result is dominated by the noise present in the data, the inversion result assuming a constant phase across the interface is unaffected. These results clearly demonstrate that regularisation based on a constant phase assumption significantly reduces the sensitivity to noise.

Synthetic measurements on a hemisphere

Even though good results are obtained by measuring on a plane parallel to the transducer surface, the reconstructions still differ significantly from the true velocity distribution. Due to practical limitations in measurement duration and sensitivity, the planar domain necessarily has a finite aperture. However, the transducer elements typically found in medical ultrasound transducers are small compared to the wavelength, resulting in a large aperture window for the radiated acoustic energy. If pressure measurements are taken along a planar domain, an inhibitively large spatial domain is required to capture all acoustic energy. This is demonstrated in figure 5, where the spatial distribution of the normalised acoustic power

transmitted by a single element transducer is shown. In the far-field, the normalised power is approximately equal to

$$P(\mathbf{r}_p) = \frac{\sum\limits_t \left[p(\mathbf{r}_p, t) \right]^2}{\max_{\mathbf{r}_p} \left\{ \sum\limits_t \left[p(\mathbf{r}_p, t) \right]^2 \right\}}. \tag{11}$$

The aperture of the parallel square used in the experiments is the gray curve projected onto the sphere, and 83.6 % of the total power is captured in this planar domain. Thus, a significant amount of power is present at large opening angles ϕ between a point of observation and the z-axis.

In addition, if measurements are performed in a planar domain, the distance between the transducer element and the pressure measurement point increases for increasing angle, and hence the pressure amplitude will decrease strongly in points corresponding to large aperture angles making the method more sensitive to noise in the data. Consequently, part of the acoustic energy is either absent or hidden in the noise in the pressure field measurement, and the reconstructed velocity distributions will be spatially smoothened [8].

When the pressure field is measured over a hemisphere with radius $a = 1.98$ mm instead, the reconstructions improve significantly. In the absence of noise, the reconstruction errors reduce to $\epsilon = 18.7$ % for unregularised CG inversion and $\epsilon = 4.2$ % for CG inversion under the assupmtion of a constant phase. When 5 % white noise is added to the pressure measurements, the reconstruction results shown in figure 6 are obtained. In this figure, the kinetic energy distribution $K(\mathbf{r}_v)$ is shown for the original and for the two reconstructed velocity distributions. Observe that almost no spatial smoothening is present in both reconstructions, and that the reconstructed transducer element oscillates with an almost spatially invariant amplitude.

In addition, observe that the reconstruction obtained using unregularised inversion is, contrary to the case of a planar pressure measurement domain shown in figure 4, virtually free from noise. This strong reduction in noise sensitivity is due to the greatly reduced measurement distance, and hence improved signal srength, under large angles in the case of a hemispherical pressure measurement domain.

For the above reconstruction, the hemisphere is divided into 1654 elements of equal area. To mimic the actual measurement performed later on, the hemisphere only extends down to an opening angle $\phi = 75°$. Note that the opening angle of the planar aperture is approximately equal to $\phi \approx 37°$.

Next, the significance of the opening angle, and hence of the acoustic energy radiated under large aperture angles, is demonstrated in the absence of noise. In figure 7 the normalised reconstruction error ϵ for both unregularised CG inversion and CG inversion when assuming a constant phase is plotted against the aperture angle ϕ. On the top axis, the fraction of the energy captured by a spherical section, $P_{\text{captured}}(\phi)/P_{\text{total}}$, is plotted against the aperture angle. From this plot it is clear that the reconstruction error decreases for increasing aperture angle, even at large aperture angles. This shows that the power radiated at large angles plays a significant role in the velocity profile reconstruction. Finally
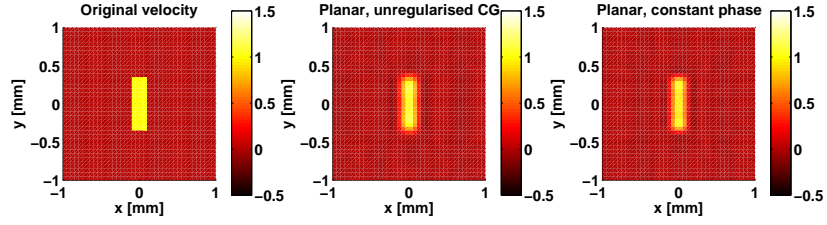
Fig. 2. A snapshot of the original time-domain velocity distribution (left), together with the time-domain results obtained from the reconstructed frequency-domain velocity distributions using unregularised CG inversion (middle) and CG inversion assuming a constant phase (right). Pressure measurements were taken in a planar domain parallel to the transducer surface. Observe that the spatial smoothening is of the same magnitude in both reconstructions. The reconstruction errors for the unregularised inversion problem and the inversion assuming a constant phase are $\epsilon = 36.0$ % and $\epsilon = 49.9$ %, respectively. Color version can be found online. **Media-color 2**
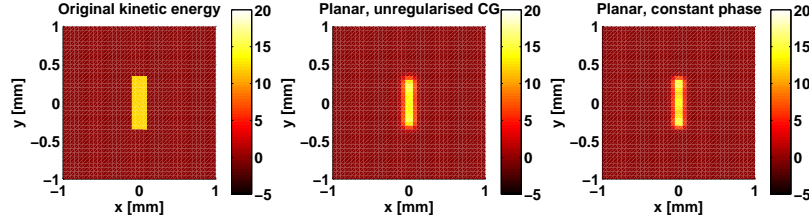
Fig. 3. The kinetic energy in $\mathbb{S}_v$ for the original velocity distribution (left), the reconstructed velocity distribution using unregularised CG inversion (middle) and CG inversion assuming a constant phase (right). Pressure measurements were taken in a planar domain parallel to the transducer surface. Both reconstructions show significant spatial smoothening, but the energy is spatially limited to the transducer element. Color version can be found online. **Media-color 3**
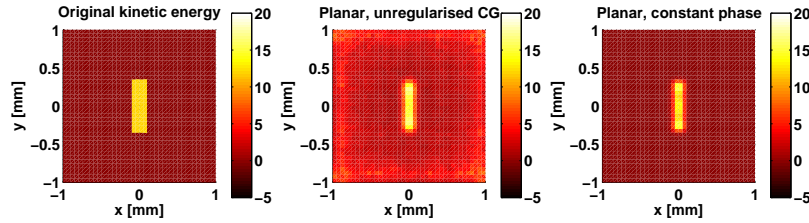

Fig. 4. The kinetic energy in $\mathbb{S}_v$ for the original velocity distribution (left), the reconstructed velocity distribution using unregularised CG inversion (middle) and CG inversion assuming a constant phase (right), in the presence of 5 % white noise added to the pressure field measurements. Pressure measurements were taken in a planar domain parallel to the transducer surface. In the case of unregularised CG inversion, the noise is overfitted to the data, resulting in a very noisy reconstruction. When a constant phase is assumed, virtually no noise is present and the reconstruction is almost identical to the noise-free situation in figure 3. Color version can be found online. **Media-color 4**

the plot shows that, for all aperture angles, the reconstruction error is lowest when assuming a constant phase.

The best achievable result obtained from pressure field measurements along the parallel plane is indicated by the gray cross in figure 7. This corresponds to capturing 83.6 % of the total power radiated by the element. Note that the reconstruction error obtained when using a spherical section capturing that same fraction of the total power is lower, which indicates that a larger measurement distance between element and hydrophone, and thus a lower signal strength, have an adverse effect on the reconstruction.

In conclusion, for the particular case studied in these synthetic experiments, the reconstruction error reduces from 36.0 % in the case of 1681 pressure measurements taken along a planar surface, to 4.2 % in the case of 1654 pressure measurements taken along a hemisphere.

B. Real measurements

For the experimental study, a linear array containing 5 elements operating at a center frequency of 12.2 MHz was built. The 200 µm kerf in between elements is filled with a dielectric for electrical insulation. The sound radiating surface of all 5 elements is covered by a monolithic matching layer. Due to the complexity of the construction, which is shown in figure 8, the exact motion of the transducer surface due to the excitation of a single element is hard to predict, but it is reasonable to assume that motion is not spatially limited to only the active element.

In this experiment, only a single element was excited by the Gaussian modulated electrical pulse of equation (8). The pulse was generated by an Agilent 33250A arbitrary waveform generator. The generated pressure field was measured using a 200 µm diameter Precision Acoustics needle hydrophone, of which the signal was amplified by +8 dB and recorded using an Agilent DSO7054A oscilloscope. The measurement domain
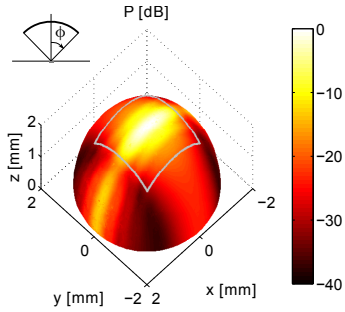
Fig. 5. The spatial distribution of the power transmitted by a transducer of dimensions 700 μm × 200 μm on a semi-sphere of radius $r = 1.98$ mm. Note that even at large aperture angles ϕ, as indicated in the sketch in the top left corner, a significant amount of power is present. The aperture of the parallel square used in the experiments is projected onto the sphere by the gray curve, and 83.6 % of the total power is captured in this planar domain. Color version can be found online. **Media-color 5**

$\mathbb{S}_p$ was scanned using an in-house built positioning system with a step size of 2.5 μm in all three directions. The same planar measurement domain as in the synthetic experiments was used. In addition, a hemisphere was traversed, but only up to $\phi = 75°$ to avoid damage to the hydrophone caused by physical contact with the array.

The kinetic energy distribution $K(\mathbf{r}_v)$ of the reconstructed velocity distributions, obtained from pressure fields measured along both a hemisphere and a planar grid, are shown in figure 9 in arbitrary units. In the top row, reconstructions from pressure measurements along a planar pressure measurement grid are shown, in the bottom row, reconstructions from pressure measurements along a hemisphere. In the left column, the unregularised CG inversion results are given, in the right column the results obtained under the constant phase assumption. The source signature $S(t)$ is estimated from the unregularised CG inversion result by selecting the time trace with maximum amplitude from $v_n(\mathbf{r}_v, t)$.

For this particular transducer, the actual motion of the transducer surface is unknown, and only the location of the driven element is indicated by the white dashed lines. However, synthetic studies reveal that a planar pressure measurement domain introduces spatial smoothening and hence increases the vibrating area in the reconstruction. Therefore, the smaller vibrating area found using a hemispherical pressure measurement domain is taken to be closer to reality. Hence, the same observations as made with the synthetic experiments hold, i.e., using a hemispherical measurement grid less spatial smoothening is introduced since the vibrating region is found to be smaller, and assuming a constant phase further reduces the energy spread. Note that a vibrating area is found of dimensions agreeing with the design to within one grid element, thus to within 50 μm, of the actual element design. Furthermore, for this transducer element, the active area is found to be slightly smaller than the designed element dimensions.

However, two unexpected phenomena occur. First, apart from the actual element, another, separate region is found to vibrate when using unregularised CG inversion. After examination under a microscope it appeared that part of the piezo electric material was erroneously electrically connected and

hence acted as a second source. Especially in the reconstruction obtained using a hemispherical pressure measurement grid, it is visible that this second region is separated from the main element, as it is in reality, see figure 8.

Second, this additional vibrating region does not show up in the reconstructions when a constant phase is assumed. Due to details in the construction, this area responds differently to electric excitation, and therefore vibrates with a different source signature $S(t)$. In addition, the region is out of phase with the actual element. Since the constant phase assumption does not hold, the vibration of this additional region is not accurately reconstructed.

IV. DISCUSSION

The Rayleigh operator $\mathcal{R}(\mathbf{r}_v, \mathbf{r}_p, \omega)$ computes the pressure field given a velocity distribution $v_n(\mathbf{r}_v, \omega)$. For accurate pressure fields, a dense spatial sampling is required. In this work, however, the velocity distribution is sampled only once per 50 μm, which amounts to 2.5 points per wavelength. To improve on the accuracy of the forward Rayleigh operator, ideally the number of points per wavelength should be significantly larger. Alternatively, the pressure contribution from each point in $\mathbb{S}_v$ could be computed using an impulse response method. However, both these approaches are computationally inhibitively expensive.

Pressure measurements are ideally taken with point-like hydrophones, both to avoid spatial averaging of the pressure field along its surface and to ensure that the hydrophone is equally sensitive in all directions. However, current commercial hydrophones typically have diameters of 200 μm or more, which is comparable to or larger than the wavelengths and element sizes studied in this work. Contrary to analytic methods using, e.g., Weyl's representation of the Green's function, the iterative approach allows both aspects, i.e., hydrophone size and radiation pattern, to be taken into account.

Although incorporating the sensitivity pattern of the hydrophone is feasible, modelling a hydrophone is non-trivial, as the construction of the hydrophone is in most cases unknown, and its mechanical behaviour may not be straightforwardly determined. Experiments not treated here show that assuming the employed needle hydrophone to be point-like, i.e., with angle independent sensitivity and no spatial averaging, yields velocity profiles that are closer to reality than when piston behaviour is assumed. Since the effect of a directivity pattern can be pronounced, the directivity should only be included if it is accurately known.

Only planar and spherical domains, both in the far-field, were studied. However, any geometry can be used, and other geometries might turn out to be advantageous. For instance, instead of a sphere, an ellipsoid can be used. In this case the distance between the active element and pressure measurement point can be smaller, and hence the signal-to-noise ratio higher. The best reconstructions are expected when the largest fraction of the radiated acoustic energy is captured by the chosen domain.

In practice, the constant phase assumption can only be made for single elements, or for arrays with identical elements.
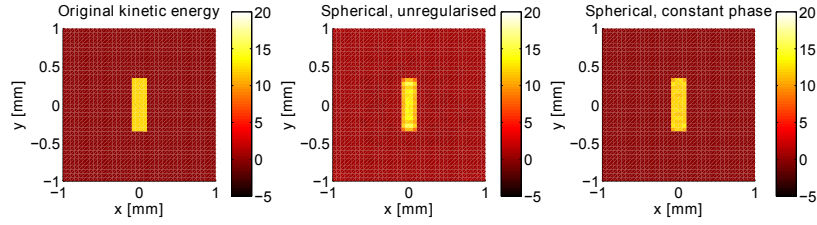
Fig. 6. The kinetic energy in $\mathbb{S}_v$ for the original velocity distribution (left), the reconstructed velocity distribution using unregularised CG inversion (middle) and CG inversion assuming a constant phase (right). Pressure measurements were taken over a hemisphere, and 5 % white noise was added to the pressure field. In both reconstructions, the kinetic energy is confined to a region of the same dimensions as the transducer element, and the spatial smoothening observed in figure 3 is significantly reduced, especially when assuming a constant phase. Observe that the noise sensitivity of especially the unregularised inversion method is significantly reduced compared to the case of a planar pressure measurement domain shown in figure 4. Color version can be found online. **Media-color 6**
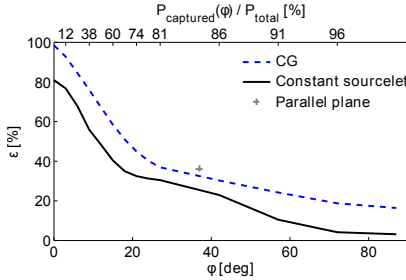

Fig. 7. Reconstruction error ϵ against the aperture angle ϕ for both unregularised CG inversion and CG inversion when assuming a constant phase. Observe that the reconstruction error decreases significantly even at high aperture angles. On the top axis, the fraction of the power captured by a sphere section is shown as a function of the aperture angle. The gray cross represents the best reconstruction result obtained from pressure measurements along the parallel plane.
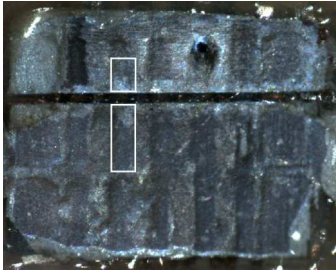

Fig. 8. Microscopic image of the transducer array. In white, the active element (bottom) and an erroneously electrically connected region of piezoelectric material (top) are indicated. The horizontal dark line is a saw cut separating the active areas from the bulk material.

Due to minor differences in construction between different elements, the mechanical behaviour of the various elements may differ, and hence the response to an electrical excitation may not be the same for different elements. For these arrays, problems may arise, as is shown in figure 9, where it is shown that velocity distributions with a spatially varying source signature are not accurately reconstructed.

In addition, in synthetic experiments not shown here it was found that areas oscillating with an identical source signature, but with different phase, are not reconstructed either. In fact, these areas are absent in the reconstruction. Therefore, for transducer arrays composed of dissimilar elements, and for
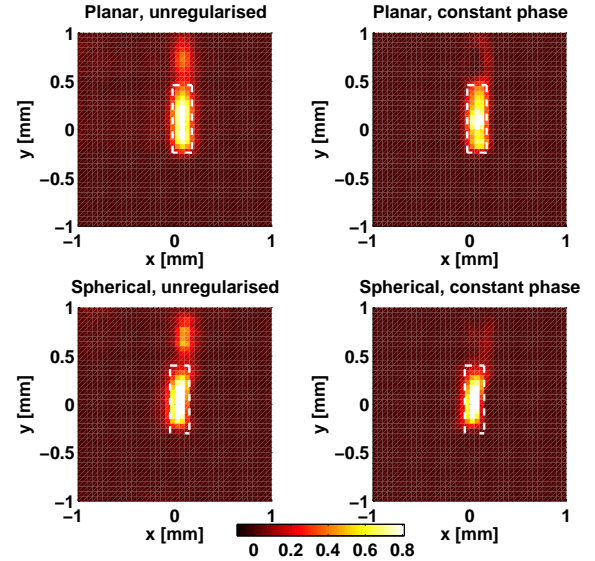

Fig. 9. The kinetic energy content, in arbitrary units, in velocity distribution reconstructions from real pressure field measurements on a parallel plane (top row) or on a hemisphere (bottom row). The dimensions of the physical element are indicated by the white lines. The reconstructions from spherical measurements consistently yield smaller vibrating regions that are closer in dimensions to the actual element size. The region around $x = 0.1$ mm, $y = 0.7$ mm originates from a part of the transducer that is erroneously electrically connected. This part of the transducer vibrates with a different sourcelet and hence is not accurately reproduced when the constant phase assumption is made. Color version can be found online. **Media-color 9**

phased or focussed arrays, either the unregularised CG scheme should be applied, or different regularisation techniques should be developed.

V. CONCLUSION

A method is presented that reconstructs the velocity distribution of the surface of an ultrasound transducer from pressure field measurements. The method employs a conjugate gradient inversion scheme to solve the Rayleigh integral of the first kind, which relates an unknown velocity distribution to a known pressure field measurement. In this work, only velocity distributions defined on a planar domain are considered, and pressure field measurements are performed on either a planar domain parallel to the transducer surface, or a hemispherical

domain. However, both the velocity distribution and pressure field measurements can be defined on arbitrarily shaped domains.

The results show that significantly more accurate reconstructions are obtained when a hemispherical pressure measurement domain is used. The improvement is caused by the fact that, using a hemisphere, all radiated acoustic energy is captured, whereas in the case of a finite planar domain, part of the energy propagates outside of the aperture. In synthetic experiments, using the same number of pressure measurements and the same measurement distance, the error in the resulting velocity distribution decreases from 36 % in the planar case to 4.2 % in the semi-spherical case.

In addition, the iterative inversion scheme allows for the application of regularisation techniques. For instance, when the assumption is made that all vibrating points on the transducer surface oscillate in phase with the same source signature, but with a spatially varying amplitude, the inverse extrapolation results further improve and spatial smoothening, in both synthetic and real experiments, is reduced. Consequently, the overestimation of cross-talk observed especially in the case of a planar pressure measurement domain is diminished. However, results show that this assumption is only valid for a single element transducers or for arrays with identical elements, as areas that vibrate with a different source signature are not well reconstructed.

Using the method, accurate velocity distribution reconstructions with resolutions down to 50 μm are obtained for a transducer element of dimensions 700 μm × 200 μm operating at a center frequency of 12.2 MHz. The measurements were performed using a needle hydrophone with a diameter of 200 μm, positioned 1.98 mm (= 16 wavelengths) away from the transducer.

References

[1] S.W. Smith, G.E. Trahey, and O.T. Von Ramm. Two-dimensional arrays for medical ultrasound. *Ultrason Imag*, 14(3):213–233, 1992.

[2] J.V. Hatfield, N.R. Scales, A.D. Armitage, P.J. Hicks, Q.X. Chen, and P.A. Payne. An integrated multi-element array transducer for ultrasound imaging. *Sensor Actuator Phys*, 41(1-3):167–173, 1994.

[3] N. Chang, D.P. Billington, and D.A. Nagy. Effect of accelerometer mass on the flexural motion of plates. *Int J Solid Struct*, 14(10):851–860, 1978.

[4] N. Yoshida. Laser Doppler velocimeter. In David Havelock, Sonoko Kuwano, and Michael Vorländer, editors, *Handbook of Signal Processing in Acoustics*, pages 1329–1338. Springer, New York, 2008.

[5] H. Weyl. Ausbreitung elektromagnetischer Wellen über einem ebenen Leiter. *Ann Phys*, 365(21):481–500, 1919.

[6] G.C. Sherman, A.J. Devaney, and L. Mandel. Plane-wave expansions of the optical field. *Optic Comm*, 6(2):115–118, 1972.

[7] W.A. Veronesi and J.D. Maynard. Nearfield acoustic holography (NAH) II. Holographic reconstruction algorithms and computer implementation. *J Acoust Soc Am*, 81(5):1307–1322, 1987.

[8] E.J. Alles, M.D. Verweij, and K.W.A. Van Dongen. Reconstructing transducer surface motion by inverse extrapolation of measured pressure wavefields. In *IEEE International Ultrasonics Symposium*, pages 1458–1461, San Diego, CA, 2010. IEEE.

[9] E.J. Alles, M.D. Verweij, and K.W.A. Van Dongen. Iterative inverse extrapolation for transducer characterization. In *IEEE International Ultrasonics Symposium*, pages 369–372, Orlando, FL, 2011. IEEE.

[10] O.A. Sapozhnikov, Y.A. Pishchalnikov, and A.V. Morozov. Reconstruction of the normal velocity distribution on the surface of an ultrasonic transducer from the acoustic pressure measured on a reference surface. *Acoust Phys*, 49(3):354–360, 2003.

[11] O.A. Sapozhnikov, A.V. Morozov, and D. Cathignol. Piezoelectric transducer surface vibration characterization using acoustic holography and laser vibrometry. In *IEEE International Ultrasonics Symposium*, pages 161–164, Montral, Canada, 2004. IEEE.

[12] P.R. Stepanishen and K.C. Benjamin. Forward and backward projection of acoustic fields using fft methods. *J Acoust Soc Am*, 71(4):803–812, 1982.

[13] E.G. Williams, H.D. Dardy, and K.B. Washburn. Generalized nearfield acoustical holography for cylindrical geometry: Theory and experiment. *J Acoust Soc Am*, 81(2):389–407, 1987.

[14] M.E. Schafer and P.A. Lewin. Transducer characterization using the angular spectrum method. *J Acoust Soc Am*, 85(5):2202–2214, 1989.

[15] A. Yaghjian. An overview of near-field antenna measurements. *IEEE Trans Antenn Propag*, 34(1):30–45, 1986.

[16] E.G. Williams. Regularization methods for near-field acoustical holography. *J Acoust Soc Am*, 110(4):1976–1988, 2001.

[17] M.R. Bai. Application of bem (boundary element method)-based acoustic holography to radiation analysis of sound sources with arbitrarily shaped geometries. *J Acoust Soc Am*, 92(1):533–549, 1992.

[18] N. Valdivia and E.G. Williams. Implicit methods of solution to integral formulations in boundary element method based nearfield acoustic holography. *J Acoust Soc Am*, 116(3):1559–1572, 2004.

[19] N. Valdivia and E.G. Williams. Krylov subspace iterative methods for boundary element method based near-field acoustic holography. *J Acoust Soc Am*, 117(2):711–724, 2005.

[20] E.G. Williams, B.H. Houston, P.C. Herdic, ST Raveendra, and B. Gardner. Interior near-field acoustical holography in flight. *J Acoust Soc Am*, 108(4):1451–1463, 2000.

[21] Y.T. Cho, J.S. Bolton, and J. Hald. Source visualization by using statistically optimized near-field acoustical holography in cylindrical coordinates. *J Acoust Soc Am*, 118(4):2355–2364, 2005.

[22] M. Eller and N.P. Valdivia. Acoustic source identification using multiple frequency information. *Inverse Probl*, 25(11):5–24, 2009.

[23] A.J. Berkhout. *Applied Seismic Wave Theory*. Elsevier, Amsterdam, 1987.

[24] J.R. Shewchuk. *An introduction to the conjugate gradient method without the agonizing pain*. http://www.cs.cmu.edu/ quake-papers/painless-conjugate-gradient.pdf, Cambridge, MA, 1994.

[25] P.C. Hansen. *Discrete Inverse Problems: Insight and Algorithms*. SIAM, Philadelphia, 2010.

[26] S. Osher and L.I. Rudin. Feature-oriented image enhancement using shock lters. *SIAM J Numer Anal*, 27(4):919–940, 1990.

[27] L.I. Rudin, S. Osher, and E. Fatemi. Nonlinear total variation based noise removal algorithms. *Phys Nonlinear Phenom*, 60(1-4):259–268, 1992.

[28] K.W.A. Van Dongen and W.M.D. Wright. A full vectorial contrast source inversion scheme for three-dimensional acoustic imaging of both compressibility and density proles. *J Acoust Soc Am*, 121(3):1538–1549, 2007.

E.J. Alles received his M.Sc. degree in applied physics at Delft University of Technology, the Netherlands. In 2007, he became a Ph.D. student in the Laboratory of Acoustical Wavefield Imaging at the same university. Since 2012 he is a postdoctoral researcher at the Institute of Cancer Research, Sutton, United Kingdom.

K.W.A. van Dongen received his M.Sc. degree in physics at Utrecht University, the Netherlands. From 1998 to 2002, he worked as a scientist at T&A Survey in Amsterdam, resulting in a PhD degree (2002) at Delft University of Technology. Next, he worked as a postdoctoral researcher in the Laboratory of Electromagnetic Research at the same university (2002-2003) and in the Ultrasonic Research Group, University College Cork, Ireland (2003-2005). In 2006 he returned to Delft University of Technology.